Study on Support-free Printing of Large-flow Material Extrusion Process

Huaying Wu (wuhy@mail.xjtu.edu.cn)
Xi'an Jiaotong University
Xiao Wang
Yuqiang Li

Research Article

Keywords: Support-free, Large-flow, Material extrusion, Quantitative fusing segment, Air cooling

Posted Date: February 3rd, 2022

DOI: https://doi.org/10.21203/rs.3.rs-1279327/v1

Version of Record: A version of this preprint was published at The International Journal of Advanced Manufacturing Technology on March 2nd, 2023. See the published version at https://doi.org/10.1007/s00170-023-11119-4.

Abstract

Support-free printing is one of the research hotspots of material extrusion process. During the large extrusion flow printing, if there is no support, when printing bridge or suspended structure, the sagging of material probably cause printing failure due to the large weight of extrusion part and its fusion state. If the support is added, it will be very difficult to remove due to its large adhesion with the matrix. Therefore, large extrusion flow printing process is more willing to print structures without support, the large and complex structures are often difficult to print. In order to realize support-free printing of bridge structure, this paper defines a concept of quantitative fusing segment and analyzes its dynamic balance characteristics during the pellet extrusion printing process. Then the printing speed reduction and air cooling scheme according to the analysis conclusion is put forward, and the experimental verification is carried out. The results show that the sag deformation of bridge structure can be reduced effectively. This will provide some theoretical and experimental support for large-flow support-free printing.

1 Introduction

Material extrusion process based 3D-printing is becoming increasingly popular due to its low-cost and simple operation and maintenance. But it suffers from an inherent printing limitation where it cannot produce overhanging surfaces of non-trivial size. This limitation can be handled by constructing temporary support-structures, however this solution involves additional material costs, longer print time, and often a fair amount of labor in removing it [1]. This support structure problem is more serious for large-flow material extrusion printing. Support-free is desired in additive manufacturing.

Object partitioning is a common way to realize support-free 3D printing [1, 2], and multi-axis printing reinforces this approach[3]. The high degree of freedom of the robotic systems allows the fabrication of complex objects without support structures [4–6], the model is decomposed into support-free parts that can be printed one by one in a collision-free sequence [7, 8]. Multiple model decomposition methods and multi-degrees of freedom 3D printers have been researched a lot. A model can be partitioned into several sub-parts using a gravity effect partition method simulating the material-falling process when the model is stacked along the Z direction [9]. Equidistant iso-polylines is obtained as gas metal arc welding path by using geodesic distance on triangular mesh to generate a geodesic scalar field [10]. A lattice infill structure generation method is researched by considering both the self-supporting condition for the infill and the support-free requirement at the boundary surface of the part [11]. A global-optimal decomposition method for minimizing the surface area to be supported [12, 13], an accelerated decomposition algorithm based on neutral network [14], wire and arc additive manufacturing method with surface/interior separation and surface segmentation [15] etc. The support-free printing methods mentioned above require rapid cooling of extruded materials, otherwise they will sag due to the gravity.

In addition to multi-axis motion printing, there are some other methods for support-free printing. Some methods start with material research. Self-healing materials can also realize free-standing seamless large-scale 3D printing [16]. Self-healing materials can be printed with modular designs capable of

healing together to form highly complex and large parts [17]. Some methods start with structural avoidance at the beginning of model design. An vertically arranged long ellipsoids can be used to realize support-free hollowing 3D printing [18]. An overhang angle constrained algorithm is used in model design to avoid the possible support demand risk [19]. There is also a way to try to replace the solid force with the levitation force, and it is possible to realize support-free printing by using ultrasonic levitation force instead of supporting structure [20].

The Large Scale Additive Manufacturing (LSAM) of 3D printing of polymers is a commercial production field emerging from its infancy [21]. It has a large extrusion flow per unit of time. LSAM of thermoplastic material requires some new design ideas compared to Small Scale Additive Manufacturing (SSAM) to create large-scale parts. For large-scale printing, the research contents are generally in thermal analysis [22], mechanical properties [23], characterizing material transitions [24], process simulation [25], fiber orientation analysis [26], extrusion control [27] and layer time control [28] etc. LSAM stays hotter than SSAM for a longer period of time. This facilitates interlayer diffusion and weld formation, but can also lead to slumping or sagging [29]. To avoid slumping of overhanging features, the thermal profiles of large printed parts have been experimentally measured and mathematically modeled [30]. In large area pellet extrusion additive manufacturing, the temperature of the substrate just before the deposition of a new subsequent layer affects the overall structure of the part [31].So the temperature is one of the key parameters. As hot plastic is extruded over a large gap, small printers can bridge gaps of several inches, however on the LSAM system, it will sag and break off due to the increased weight and temperature [32]. At present, the bridge or overhanging structures are avoided as far as possible in the printing process of LSAM system, and how to solve their sagging problem is rarely mentioned. This will limit the shape of the parts that can be printed.

If the bridge structure of the first layer is printed without support, it can be used as the support of subsequent layers. Therefore, the realization of support-free printing of the first layer bridge structure is the most important. This paper studies the effect of rapid cooling on preventing large-flow material sagging when printing first layer bridge structure in LSAM system.

2 Fused Deposition Analysis Model

In this paper, the large flow printing process is described in Fig. 1. First, the material is extruded out from the print head in direction *y*. Second, the material is deposited on the former layer along *x* direction. The material extruded from the print head will change from section A to section B, and they are equal in volume. The printing process can be described as the dynamic continuous transformation of section A material into section B material with a more fixed geometry. If all relevant external conditions remain unchanged, this stable transformation will continue. So section A is defined as Quantitative Fusing Segment (QFS). In order to ensure the quality of the printed parts, the extrusion material deposited at the same distance should be consistent theoretically. Therefore, the moving speed of the print head is analyzed by the average speed *v*. With the print head moves from position 1 to position 1', the geometry of A' material should be the same as that of QFS-A.

The QFS-A and QFS-B are taken out separately for force analysis (see Fig. 1). QFS-A segment is subjected to the comprehensive effects of gravity *GA*, the supporting force *FA* from the former fused deposition layer, the pulling force *fAB* (internal bonding force of the material between QFS-A and QFS-B), and the pulling force *fA* (internal bonding force of the material inside the print head). QFS-B segment is subjected to the gravity *GB* = *GA*, the supporting force *FB* from the former fused deposition layer, the pulling force *fAB* and *fB* (internal bonding force). These forces are dynamically balanced during printing. The force *fAB* and *fA* are strongly correlated with the temperature, which include heating temperature of the print head, heating temperature of the worktable (if this function is available), ambient temperature of the print workspace (some workspaces have active heating function) and temperature of deposited material after extrusion. Printing process parameters such as *v* and layer thickness also affect temperature field directly. Due to the mutual heat transfer between the deposition layers and the radiation to the workspace, the temperature field of the whole printing process is complex. In order to simplify the analysis, this paper only focuses on the temperature change at QFS-A.

Under the same printing conditions, the four forces of QFS-A should remain unchanged. Thus the geometric shape of QFS-A and QFS-B are in a relatively stable state, and the printing quality is guaranteed by this dynamic equilibrium. When the temperature or support area of QFS-A changes, this dynamic balance will be broken, and the geometric shapes of QFS-A and QFS-B should be changed. This includes the following possibilities:

1) When the temperature conditions change, the internal bonding force should be changed, f_{AB} or f_A changes will make the force state of QFS-A lose dynamic balance. For large flow printing, when other process parameters remain unchanged, the change of velocity *v* is an important factor causing the change of temperature.

2) When the supporting area changes, F_A disappears, the dynamic force balance of QFS-A is seriously broken, and its geometry shape will change, then resulting in print quality problems.

3) When the temperature conditions and the supporting area are all change at the same time, f_{AB}, f_A and F_A are affected at the same time, the dynamic force balance of QFS-A will be lost immediately.

3 Large-flow Printing Experiment With Support-free

3.1 Experimental model design

In order to analyze and verify the possibility of printing with support-free, a cylindrical model with a part cut obliquely shown in figure Fig. 2 is designed. D is diameter. H and h are respectively the highest and lowest point of the oblique section on the cylinder to the bottom of the cylinder. After slicing, a variety of unsupported monofilaments with different bridge spans can be generated, and the span can be adjusted by adjusting the diameter D of the model. In this model, we can intuitively compare the deformation of monofilament with different spans.

3.2 Printing experiment

The screw extrusion printing equipment was developed by the author and her team, whose printing size is 800×600×500 (mm). It was totally enclosed and equipped with quick air cooling auxiliary components on the print head (see Fig. 3). In this way, on the one hand, the printing ambient temperature can be guaranteed to be in a relatively stable state; on the other hand, the extrusion material temperature can be adjusted as needed. The diameter of printing nozzle includes 1mm, 2.5mm and 3.5mm, and 2.5mm is adopted in this paper. The printing material used in this paper is Acrylonitrile Butadiene Styrene (ABS) pellet. The screw print head is heated in two stages, and the upper part is heated at 175°C and the lower part is heated at 200°C. The printing ambient temperature is 40°C.

The printing process parameters are set as: the layer thickness is 1.5mm and the layer width is 4mm, then the theoretical diameter of extruded monofilament is 2.76mm. The parameters of the experimental model are D=200mm, H=100mm, h=73mm.The printing speed is set to 70mm/s. The sag of unsupported suspended monofilament increases regularly with the increase of bridge span. At the maximum span of 187mm, the maximum sag deformation size is 80mm, and the monofilament almost touches the bottom of the model (see Fig. 4). The smallest diameter of the end is 1.51mm, which is only 54% of the theoretical diameter.

3.3 Analysis of experimental results

3.3.1 Mechanical State of ABS material

The ABS material used in this experiment is POLYLAC PA-757, which is an amorphous polymer. It is divided into three mechanical states according to the temperature region – glassy state, elastomeric state and viscous flow state (see Fig. 5). The glass transition temperature T_g=88℃, flow temperature T_f=190℃, the deformation of the material increases with the increase of temperature.

In the glassy state, due to the low temperature and low molecular motion energy, it is not enough to overcome the potential barrier of rotation in the main chain, and the chain segment is frozen. When subjected to external force, only the bond length and bond angle of the main chain can be slightly changed. Therefore, from a macro perspective, the deformation of polymer under external force is very small, and it is directly proportional to the force. When the external force is removed, the deformation energy recovers immediately. At this time, ABS is in a state of general elasticity, and the deformation is 0.01% - 0.1%.

In the elastomeric state, the energy of molecular thermal motion is enough to overcome the potential barrier of internal rotation. The molecule continuously changes the conformation through the internal rotation of the single bond in the main chain. At this time, the chain segment motion is excited, when ABS is subjected to external force, the molecular chain can change the conformation through the internal rotation of the single bond and the chain segment to adapt to the action of it. For example, when ABS is subjected to tensile force, the molecular chain can change from the curled state to the extended state, so

great deformation can occur macroscopically. Once the external force is removed, the molecular chain will return to the original curled state through the internal rotation of the single bond and the motion of the chain segment, which is shown as elastic retraction in the macro. Because this deformation is a process of internal rotation of the polymer main chain caused by external force, the external force required is obviously much smaller than that required for the deformation of the polymer in the glassy state, but the amount of deformation is much larger, and the high elastic deformation is about 100% - 1000%.

In the viscous flow state, the relaxation time of chain segment movement continues to shorten, and the relaxation time of the whole molecular chain movement also shortens. At this time, the polymer will have viscous flow under the action of external force, which is the macro manifestation of the mutual sliding of the whole molecular chain. This state is similar to the flow of low molecular liquid. It is irreversible deformation. After the external force is removed, the deformation can no longer recover spontaneously.

3.3.2 Temperature field of suspended monofilament printing

The temperature distribution on the suspended monofilament with the largest span is shown in Fig. 6. The temperature in QFS-A at the right end of the suspended monofilament is 211.3℃, in QFS-B is 207.3℃, and the farther away from the print head, the lower the temperature. The temperature at the center of the monofilament is 184.5℃, and the lowest temperature at the left end of the monofilament is 147.3 ℃, but the temperature of the cylindrical part connected with it is 189.2 ℃. This shows the left half of the monofilament cools faster, because the cooling time of the left half is longer and the material of the left half is less than that of the right half. And the temperature of the former layer has a great influence on this layer.

3.3.3 Deformation analysis of suspended monofilament

1) Thermal deformation analysis of monofilament

The suspended printed monofilament is taken out separately for analysis (see Fig. 7). It can be judged from the T_g and T_f of ABS that the temperature at the L circle is close to T_f, and the temperature in the R circle is above T_f. For the suspended monofilament, the deformation at these two positions is the most serious. The temperature in other places on the monofilament is between T_g and T_f. Therefore, under the force of gravity, the whole ABS material deforms large, and the material easily flows at both ends. The deformation is irreversible. Before the temperature drops to T_g, this deformation will last for a long time because gravity will not disappear. With the increase of bridge span, the weight of monofilament will also increase and the deformation will be more serious. Moreover, since there is no additional material, the junction between the left end and the cylindrical part will become a fracture risk.

2) Analysis of QMS

The model shown in Fig. 2 can print bridge structures with free support. When the moving direction of the print head changes from circle to line, it can be inferred from Fig. 1 that the speed v changes, the support force FA disappears, then geometric instability of QFS-A will be occurred obviously.

The force state of QFS-A is analyzed (see Fig. 8). It can be seen from Fig. 6, the temperature at f_A is higher than that at f_{AB}, so it is inferred that $f_A < f_{AB}$ according to the material characteristics. The resultant force F_1 in y direction and the total resultant force P_A are shown in formula (1) and formula (2). When F_A is canceled, F_1 becomes larger, P_A increases and its direction will tend to the gravity direction. This will improve the probability of forward transition of the chain segment in the thermoplastic polymer along the P direction. In this experiment, the temperature in QFS-A is above T_f, P_A is easy to make the material flow along it, and produce large deformation (see Fig. 4), if the materials are not supplemented in time, the cross-sectional area will be reduced and increasing the fracture risk.

$$\vec{F}_1 = \vec{G}_A - \vec{F}_A - \vec{f}_A \quad (1)$$

$$\vec{P}_A = \vec{F}_1 + \vec{f}_{AB} \quad (2)$$

The force state of QFS-B is relatively simple. If the temperature drops slowly, f_B can be considered to be the same as f_{AB}. When F_B disappears, the resultant P_B shown in formula (3) changes and the material will drop down. According to the temperature distribution in Fig. 7, in area L the force f_B will be less than f_{AB}, the resultant force will tilt downward to the right and make the material flow along this direction. In this experimental case, if you continue printing, the next layer cannot be deposited on this bridge layer due to excessive deformation.

$$\vec{P}_B = \vec{G}_B - \vec{F}_B + \vec{f}_B - \vec{f}_{AB} \quad (3)$$

It can be seen from the above analysis that in order to realize support-free printing, the deformation of monofilament can be reduced by increasing f_B, f_{AB}, or reducing G_A or G'. Lowering the temperature is an effective way to improve f_B and f_{AB}.

4 Optimization Of Reducing Sagging Deformation For Suspended Printing

4.1 Air cooling

In this paper, the extrusion nozzle is not replaced, so it is considered that the G_A of QFS-A remains unchanged. In order to increase f_{AB}, rapid cooling of QFS-A polymer material is a convenient method.

The air cooling auxiliary structure has two 7mm diameter air nozzles to input high-pressure air. The pressure of the air compressor is 7 kpa and the flux is 45 L/min. The air volume is adjusted so that it cannot affect the geometric shape of QFS-A. Other conditions and parameters remain unchanged. The final printing results are shown in Fig. 9. The sagging deformation of the same position becomes from

80mm to 38mm, which is reduced to 47.5% compared with no air cooling. And the diameter of the thinnest suspended monofilament becomes 2mm, reaching 72.5% of the theoretical diameter.

4.2 Deceleration + air cooling

According to the optimization results in Fig. 9, further improvement scheme is proposed: reduce the moving speed of the print head to 20mm/s on the basis of air cooling to lower the material temperature.

The experimental results show that, the deformation of the same position becomes 12mm, which is reduced to 15% compared with no air cooling. The diameter of the thinnest suspended monofilament becomes 2.48mm, which reaches 90% of the theoretical diameter (see Fig. 10). Obviously, improving f_{AB} is an effective and feasible method to reduce the deformation of suspended printing.

4.3 Deceleration + air cooling + span reduction

If G' is reduced by shorten the bridge span while increasing f_{AB}, it will be more conducive to the reduction of monofilament deformation. On the basis of air cooling and printing speed of 20mm/s, the model diameter is adjusted to 150mm. The maximum sag deformation of the suspended monofilament of the whole model is 5mm.The minimum diameter of one end of the monofilament is 2.52mm, reaching 91% of the theoretical diameter, and the diameter of the middle position is 2.76mm, which is the same as the theoretical diameter, while the other end is 2.79mm, which is 101% of the theoretical diameter (see Fig. 11). This means that the overall diameter error of the suspended monofilament is within 8.7%, indicating that the migration caused by the chain reaction of the material itself is greatly reduced.

The deformations at different spans are shown in Fig. 12. It can be seen that the maximum deformation of the monofilament under the 71mm span is only 3mm, which is close to the theoretical diameter of the monofilament. When printing the second layer on this monofilament, there will be more contact between the upper and lower materials (see Fig. 13). This will greatly reduce the size of the suspended span on the next layer, and make support-free printing possible.

4.4 Thermal deformation analysis

Comparing the thermal fields of the three deformation reduction schemes (see Fig. 14), when the printing speed is dropped from 70mm/s to 20mm/s under air cooling conditions, the time required for printing the same length increases, then there is more time for the material to dissipate heat. It can be seen that the overall temperature on the suspended monofilament decreases significantly. When the model diameter changes from 200mm to 150mm, although the monofilament length decreases, the temperature at similar positions on the monofilament is similar, indicating that the further decrease of monofilament deformation is mainly due to the smaller G'.

4.5 Deformation analysis

The deformation comparison at the same position of the 200mm diameter model in three states is shown in Fig. 15. The deformations under different spans are in the form of parabola. The larger the temperature

drop, the smaller the deformation; and the larger the span, the greater the deformation. The parabolic model can be derived easily by fitting the sample data, which can provide some reference for the deformation analysis of bridge structure.

5 Conclusions And Future Work

In this paper, the principle of large flow printing is analyzed, the QFS is defined, and its dynamic balance is analyzed. A possible solution for support-free printing of large flow printing is proposed and verified by experiments. The results show that the scheme of rapid cooling of QFS is conducive to improve f_{AB} and decrease the deformation of suspended monofilament. The span should be within a reasonable range, so that f_{AB}, GA and G' can achieve appropriate dynamic balance. This will help to make the sag deformation within an allowable range. If necessary, this layer will also become the support of the next layer.

In order to further explore and improve the theoretical analysis of support-free printing, the following work needs to be carried out:

1) The quick cooling structure needs to be further improved to avoid the influence of blowing QFS-A during cooling and ensure more accurate control.

2) Combined with the relationship between material heat quantity and temperature, the thermal deformation model of monofilament needs to be further studied, and the corresponding stress-heat relationship model of QFS at A and B position should be built to give a reasonable cooling rate.

3) The deformation accuracy that not affecting the next layer printing should be researched, so as to get the critical span value with different diameters for support-free printing.

Declarations

Funding

This work was supported by National Natural Science Foundation of China (Grant numbers: 51805417).

Competing Interests

The authors have no relevant financial or non-financial interests to disclose.

Author Contributions

Huaying Wu contributed to the study conception and design. Material preparation, data collection and analysis were performed by Xiao Wang and Yuqiang Li. The first draft of the manuscript was written by Huaying Wu and all authors commented on previous versions of the manuscript. All authors read and approved the final manuscript.

References

1. Karasik E, Fattal R, Werman M (2019) Object Partitioning for Support-Free 3D-Printing. Computer Graphics Forum 38(2):305–316. https://doi.org/10.1111/cgf.13639
2. Wei XZ, Qiu SQ, Zhu L, Feng RL, Tian YB, Xi JT, Zheng YY (2018) Toward Support-Free 3D Printing: A Skeletal Approach for Partitioning Models. Ieee Transactions on Visualization and Computer Graphics 24(10):2799–2812. https://doi.org/10.1109/Tvcg.2017.2767047
3. Hu QX, Cui J, Zhang HG, Liu SH, Ramalingam M (2021) A 5+1-Axis 3D Printing Platform for Producing Customized Intestinal Fistula Stents, 3d Printing and Additive Manufacturing. https://doi.org/10.1089/3dp.2021.0044
4. Urhal P, Weightman A, Diver C, Bartolo P (2019) Robot assisted additive manufacturing: A review, Robotics and Computer-Integrated Manufacturing. 59: 335-345. https://doi.org/10.1016/j.rcim.2019.05.005
5. Murtezaoglu Y, Plakhotnik D, Stautner M, Vaneker T (2018) and F. J. A. M. van Houten Geometry-Based Process Planning for Multi-Axis Support-Free Additive Manufacturing, 6th Cirp Global Web Conference - Envisaging the Future Manufacturing, Design, Technologies and Systems in Innovation Era (Cirpe 2018). 78: 73-78. https://doi.org/10.1016/j.procir.2018.08.175
6. Dai CK, Wang CCL, Wu CM, Lefebvre S, Fang GX, Liu YJ (2018) Support-Free Volume Printing by Multi-Axis Motion. Acm Transactions on Graphics 37(4). https://doi.org/10.1145/3197517.3201342
7. Wu C, Dai C, Fang G, Liu Y, Wang CCL (2017) RoboFDM: A robotic system for support-free fabrication using FDM. in 2017 IEEE International Conference on Robotics and Automation (ICRA). https://doi.org/10.1109/ICRA.2017.7989140
8. Xiao XY, Joshi S (2020) Process planning for five-axis support free additive manufacturing, Additive Manufacturing. https://doi.org/10.1016/J.Addma.2020.101569. 36 Artn 101569
9. Liu H, Liu L, Li DW, Huang RK, Dai N (2020) An approach to partition workpiece CAD model towards 5-axis support-free 3D printing. International Journal of Advanced Manufacturing Technology 106(1–2):683–699. https://doi.org/10.1007/s00170-019-04495-3
10. Liu B, Shen HY, Deng RX, Zhou ZY, Jia JA, Fu JZ (2021) Research on GMAW based non-supporting thin-wall structure manufacturing. Rapid Prototyping Journal 27(2):333–345. https://doi.org/10.1108/Rpj-05-2020-0102
11. Li Y, Tang K, He D, Wang X (2021) Multi-Axis Support-Free Printing of Freeform Parts with Lattice Infill Structures, Computer-Aided Design. 133:102986. https://doi.org/10.1016/j.cad.2020.102986
12. Gao Y, Wu L, Yan D-M, Nan L (2019) Near support-free multi-directional 3D printing via global-optimal decomposition. Graph Models 104:101034. https://doi.org/10.1016/j.gmod.2019.101034
13. Wu LF, Gao YS, Yu M, Jian M, Liu ZC, Guan YP (2018) Global-optimization-based Model Decomposition for Support-free Multi-DOF 3D Printing, Sa'18: Siggraph Asia 2018 Posters. Artn 30. https://doi.org/10.1145/3283289.3283352

14. Wu C, Liu Y, Wang CCL (2020) Learning to Accelerate Decomposition for Multi-Directional 3D Printing, IEEE Robotics and Automation Letters. 5:5897–5904. https://doi.org/10.1109/lra.2020.3011369. 4
15. Liu B, Shen HY, Zhou ZY, Jin J, Fu JZ (2021) Research on support-free WAAM based on surface/interior separation and surface segmentation. J Mater Process Technol 297. https://doi.org/10.1016/j.jmatprotec.2021.117240
16. Zuo H, Liu ZH, Zhang LZ, Liu GX, Ouyang XK, Guan QB, Wu QL, You ZW (2021) Self-healing materials enable free-standing seamless large-scale 3D printing. Science China-Materials 64(7):1791–1800. https://doi.org/10.1007/s40843-020-1603-y
17. Gomez EF, Wanasinghe SV, Flynn AE, Dodo OJ, Sparks JL, Baldwin LA, Tabor CE, Durstock MF, Konkolewicz D, Thrasher CJ (2021) 3D-Printed Self-Healing Elastomers for Modular Soft Robotics. Acs Applied Materials & Interfaces 13(24):28870–28877. https://doi.org/10.1021/acsami.1c06419
18. Choi S, Ryu J, Lee M, Cha J, Kim H, Song C, Kim DS (2020) Support-free hollowing with spheroids and efficient 3D printing utilizing circular printing motions based on Voronoi diagrams, Additive Manufacturing. 35 Artn 101254. https://doi.org/10.1016/J.Addma.2020.101254
19. Wang YG, Gao JC, Kang Z (2018) Level set-based topology optimization with overhang constraint: Towards support-free additive manufacturing. Computer Methods in Applied Mechanics and Engineering 339:591–614. https://doi.org/10.1016/j.cma.2018.04.040
20. Wu HY, Zhu JJ, Wang X, Li YQ (2021) Design of ultrasonic standing wave levitation support for three-dimensional printed filaments. J Acoust Soc Am 149(4):2848–2853. https://doi.org/10.1121/10.0003922
21. M. E. S. A. S. D.Dadmunb Role of compatibilizer in 3D printing of polymer blends,Additive Manufacturing. 27. https://doi.org/10.1016/j.addma.2019.03.009
22. Compton BG, Post BK, Duty CE, Love L, Kunc V (2017) Thermal analysis of additive manufacturing of large-scale thermoplastic polymer composites. Additive Manufacturing 17:77–86. https://doi.org/10.1016/j.addma.2017.07.006
23. Nycz A, Kishore V, Lindahl J, Duty C, Carnal C, Kunc V (2020) Controlling substrate temperature with infrared heating to improve mechanical properties of large-scale printed parts *,Additive Manufacturing. 33. https://doi.org/10.1016/j.addma.2020.101068
24. Brackett J, Yan YZ, Cauthen D, Kishore V, Lindahl J, Smith T, Sudbury Z, Ning HB, Kunc V, Duty C (2021) Characterizing material transitions in large-scale Additive Manufacturing, Additive Manufacturing. 38. https://doi.org/10.1016/j.addma.2020.101750
25. Brenken B, Barocio E, Favaloro A, Kunc V, Pipes RB (2019) Development and validation of extrusion deposition additive manufacturing process simulations. Additive Manufacturing 25:218–226. https://doi.org/10.1016/j.addma.2018.10.041
26. Wang ZG, Smith DE (2019) Numerical analysis of screw swirling effects on fiber orientation in large area additive manufacturing polymer composite deposition. Composites Part B-Engineering 177. https://doi.org/10.1016/j.compositesb.2019.107284

27. Chesser P, Post B, Roschli A, Carnal C, Lind R, Borish M, Love L (2019) Extrusion control for high quality printing on Big Area Additive Manufacturing (BAAM) systems, Additive Manufacturing. 28:445-455, https://doi.org/10.1016/j.addma.2019.05.020
28. Wang FF, Fathizadan S, Ju F, Rowe K, Hofmann N (2021) Print Surface Thermal Modeling and Layer Time Control for Large-Scale Additive Manufacturing. IEEE Trans Autom Sci Eng 18(1):244–254. https://doi.org/10.1109/TASE.2020.3001047
29. D'Amico T, Peterson AM (2020) Bead parameterization of desktop and room-scale material extrusion additive manufacturing: How print speed and thermal properties affect heat transfer. Additive Manufacturing 34. https://doi.org/10.1016/j.addma.2020.101239
30. Choo K, Friedrich B, Daugherty T, Schmidt A, Patterson C, Abraham MA, Conner B, Rogers K, Cortes P, MacDonald E (2019) Heat retention modeling of large area additive manufacturing,Additive Manufacturing. 28:325–332. https://doi.org/10.1016/j.addma.2019.04.014
31. Trejo EM, Jimenez X, Billah KMM, Seppala J, Wicker R, Espalin D (2020) Compressive deformation analysis of large area pellet -fed material extrusion 3D printed parts in relation to in situ thermal imaging *. Additive Manufacturing 33. https://doi.org/10.1016/J.Addma.2020.101099
32. Alex Roschli KTG, AM, Boulger, Brian K, Post PC, Chesser, Lonnie FB, Love J, Michael Borish (2019) Designing for Big Area Additive Manufacturing, Additive Manufacturing. 25:275-285, https://doi.org/10.1016/j.addma.2018.11.006
33. He Manjun ZH, Weixiao C, Dong Xixia (2007) Polymer Physics. Fudan University Press, Shanghai

Figures

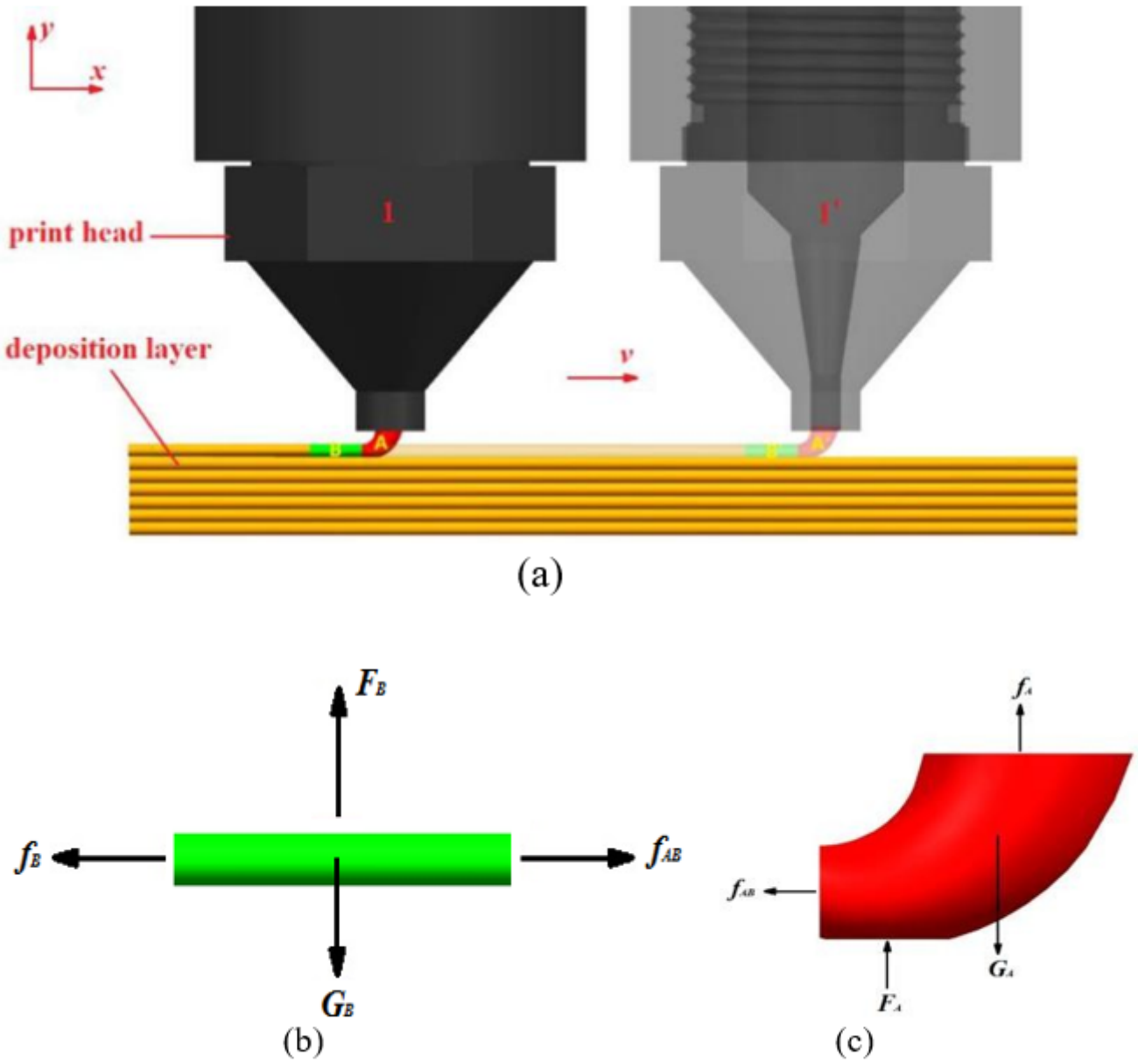

Figure 1

a Two positions of print head during fused deposition process. **b** The force state of QFS-A material. **c** The force state of QFS-B material.

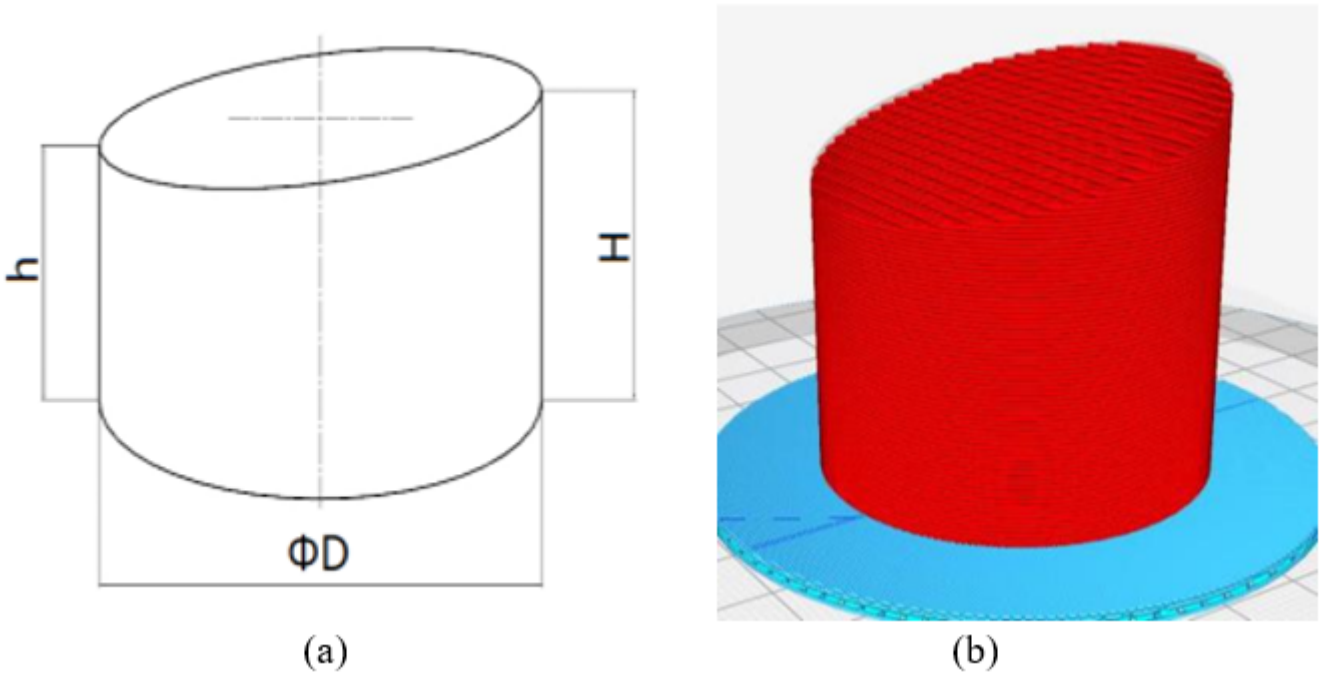

Figure 2

a Diagrammatic sketch of the Experimental model. **b** The model's structure after slicing.

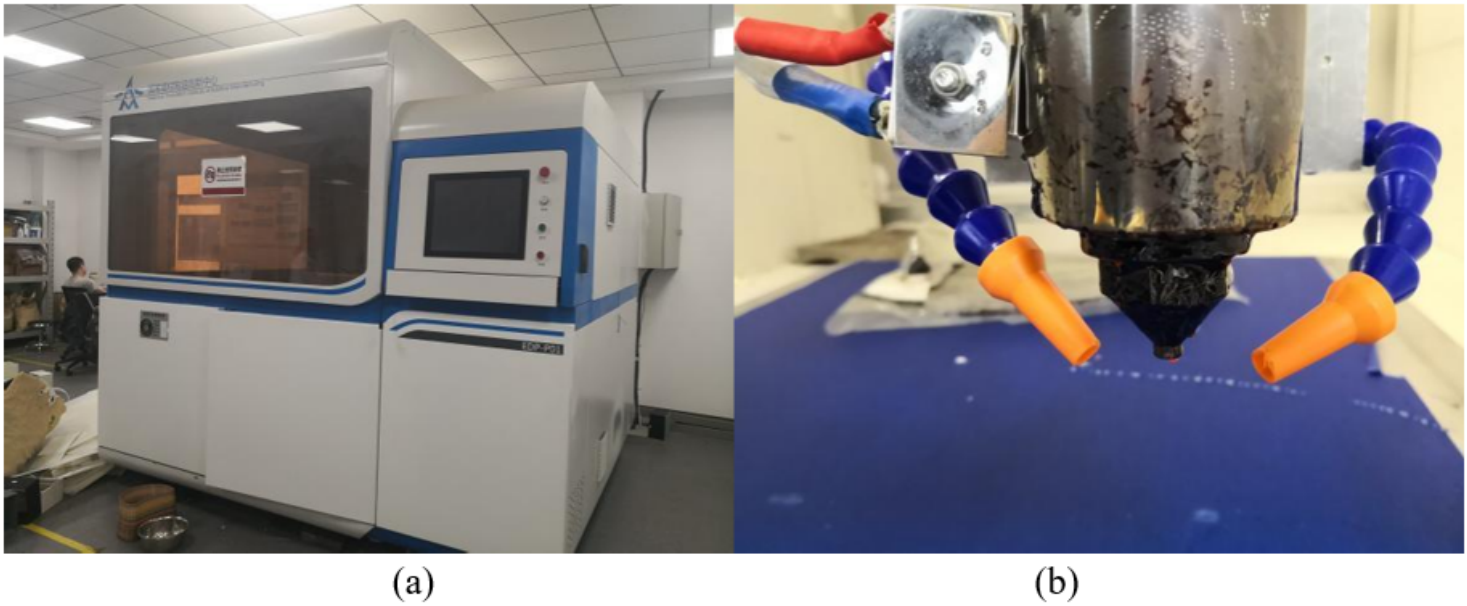

Figure 3

a Experimental equipment. **b** Auxiliary air cooling components.

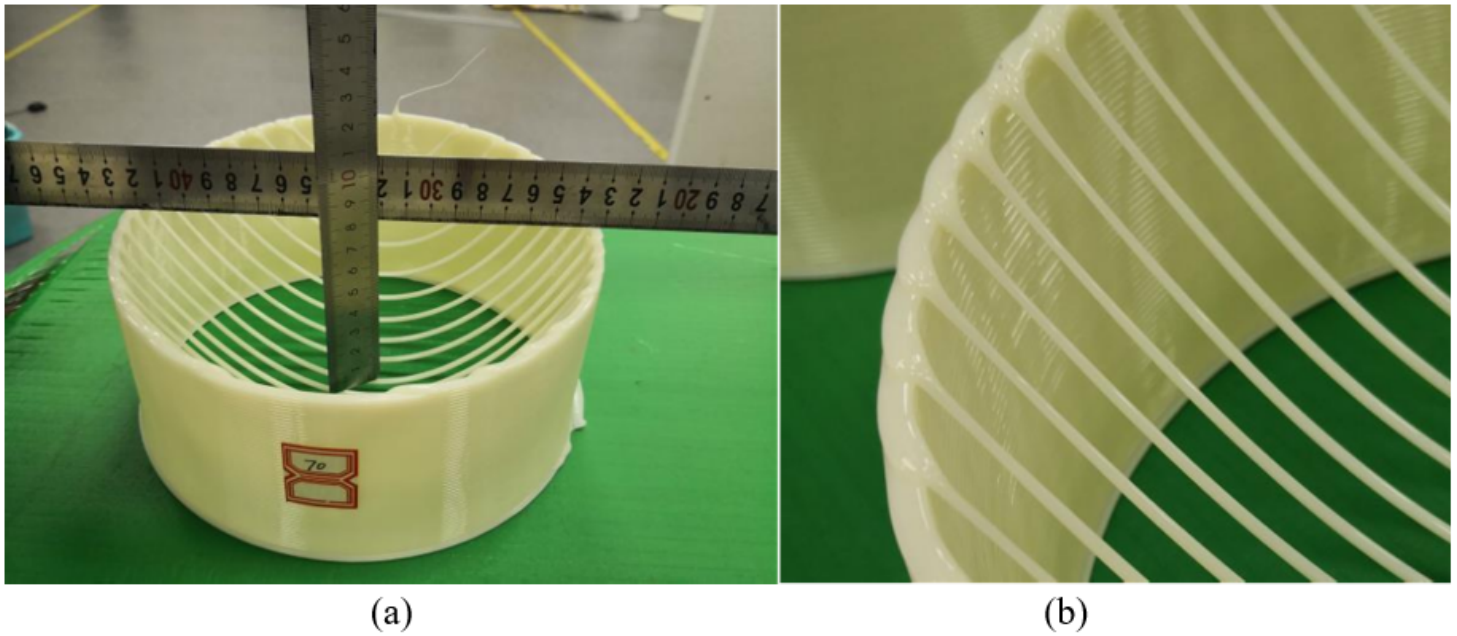

Figure 4

a The deformation of monofilament under bridge span. **b** The diameter at the end becomes thinner.

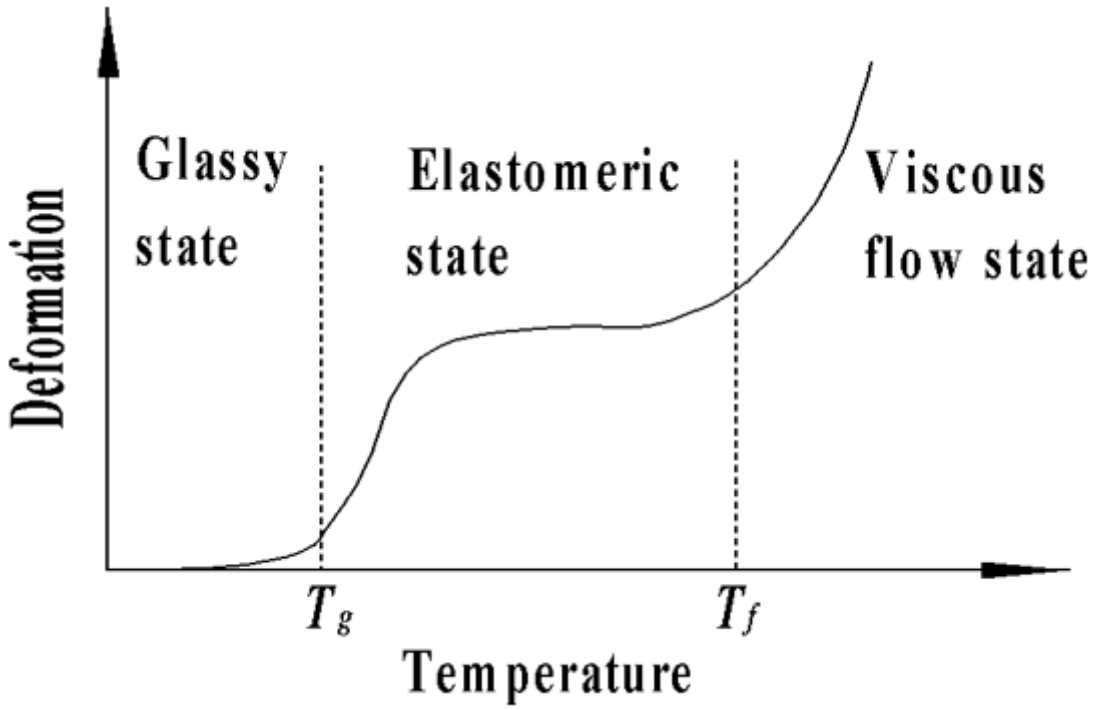

Figure 5

Relation curve between temperature and deformation of amorphous polymer [33].

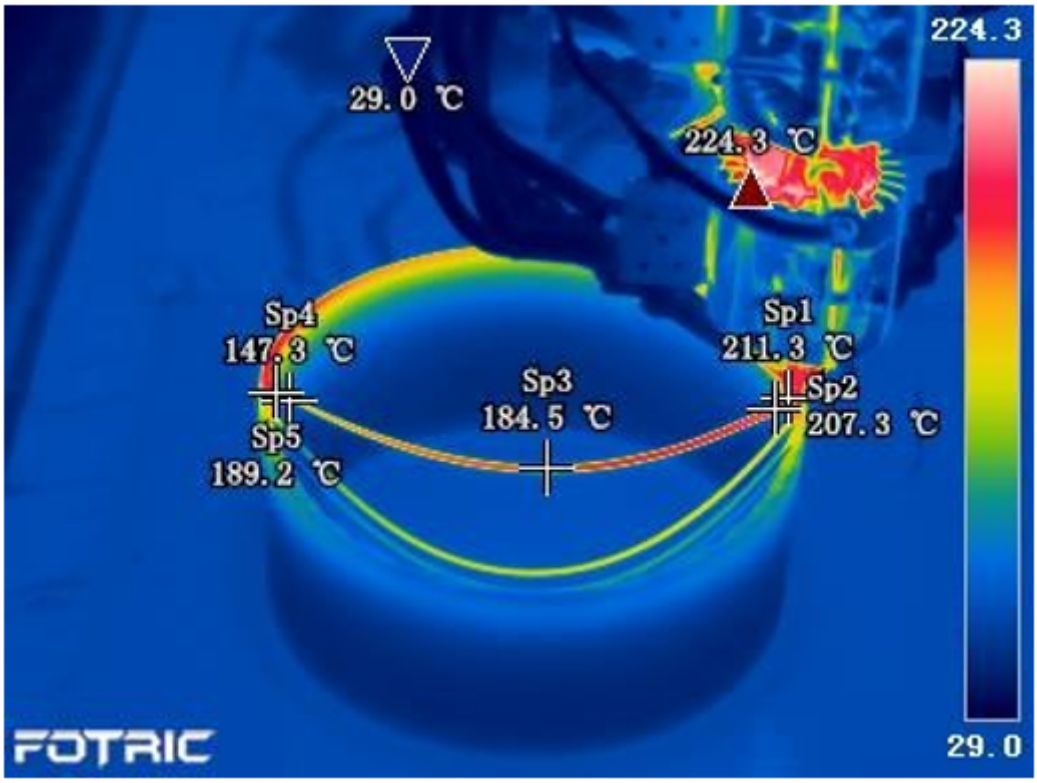

Figure 6

Temperature Field D=200mm v=70mm/s non-air cooling

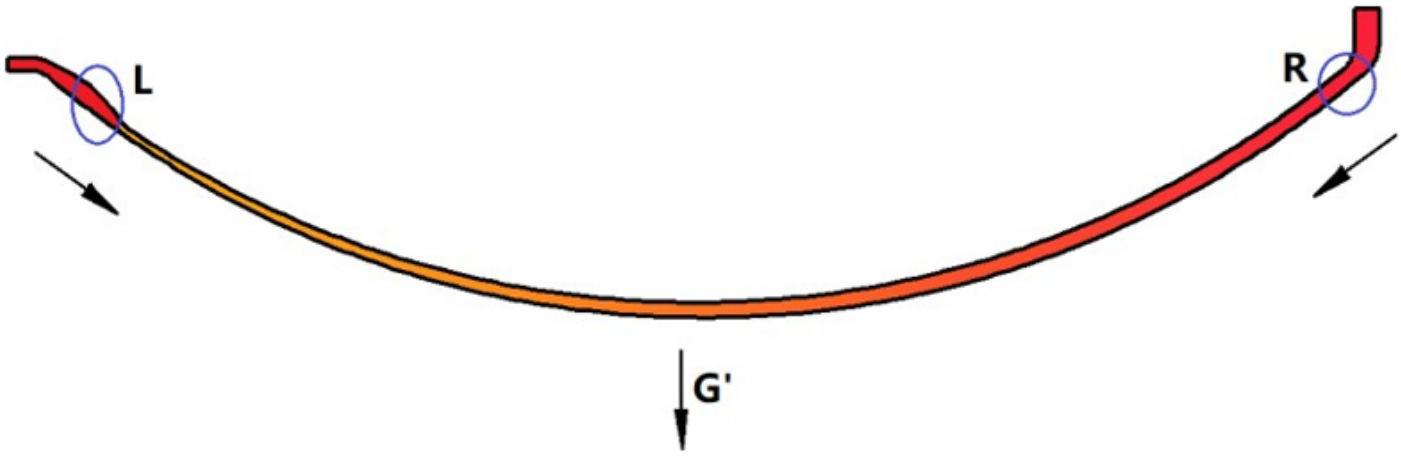

Figure 7

Sagging of suspended monofilament in hot state

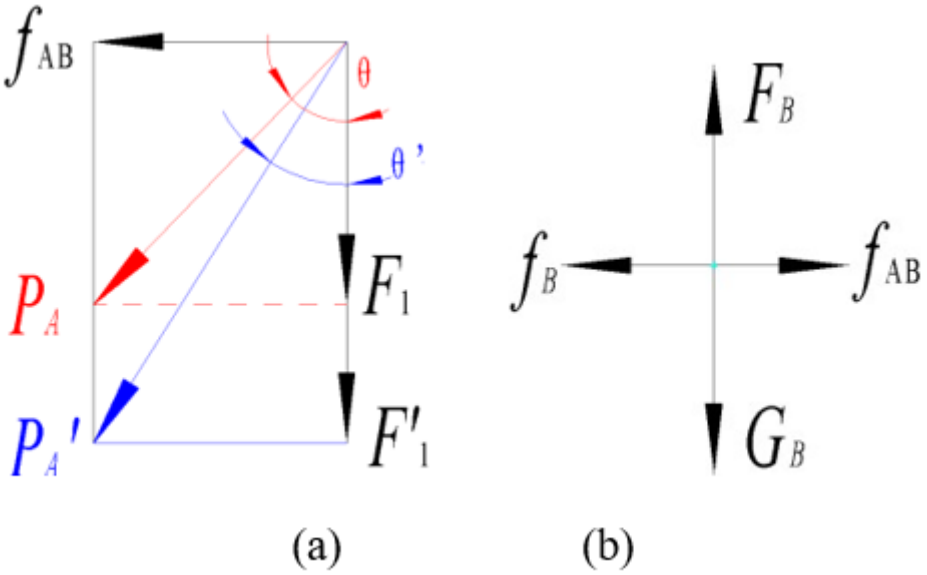

Figure 8

a Force state of QFS-A. **b** Force state of QFS-B.

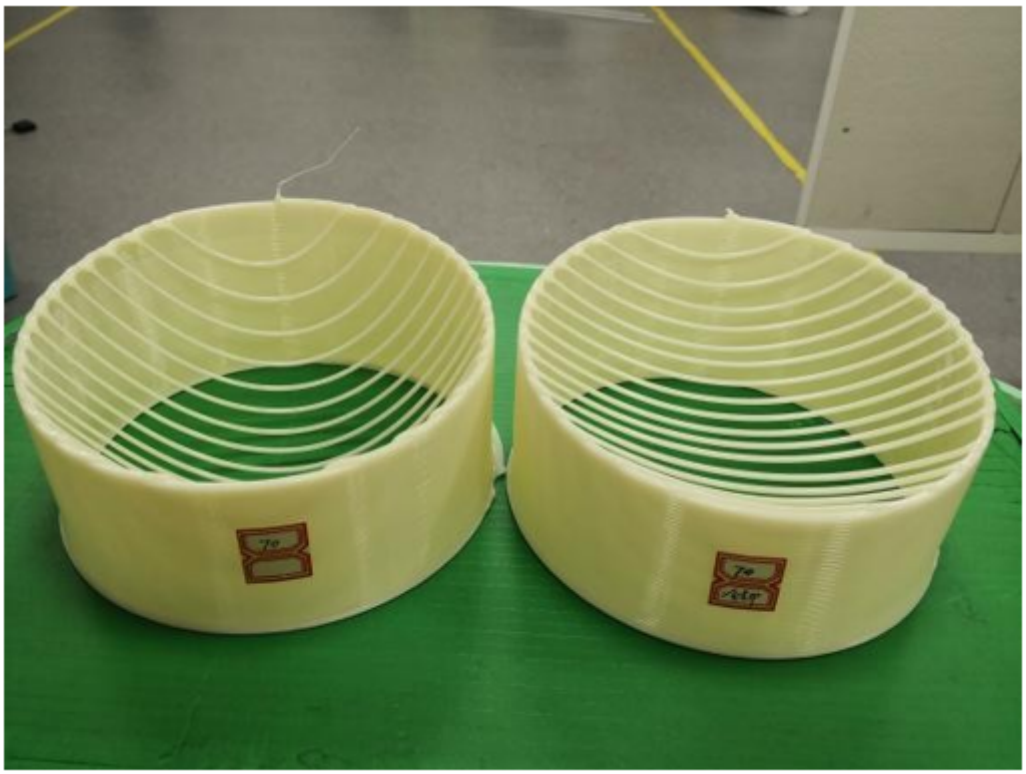

Figure 9

Comparison of Suspension Deformation before and after air cooling

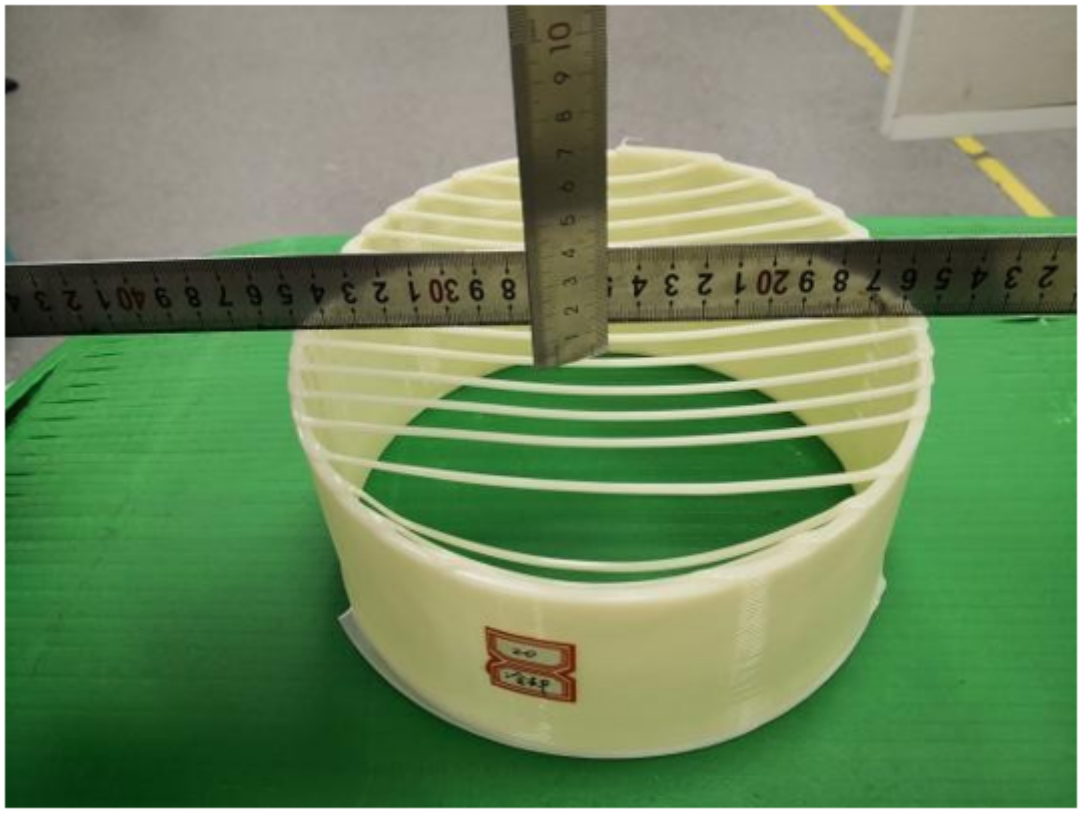

Figure 10

The deformation of monofilament under large span (D=200mm,v=20mm/s,air cooling)

Figure 11

The deformation of monofilament under large span (D=150mm,v=20mm/s,air cooling)

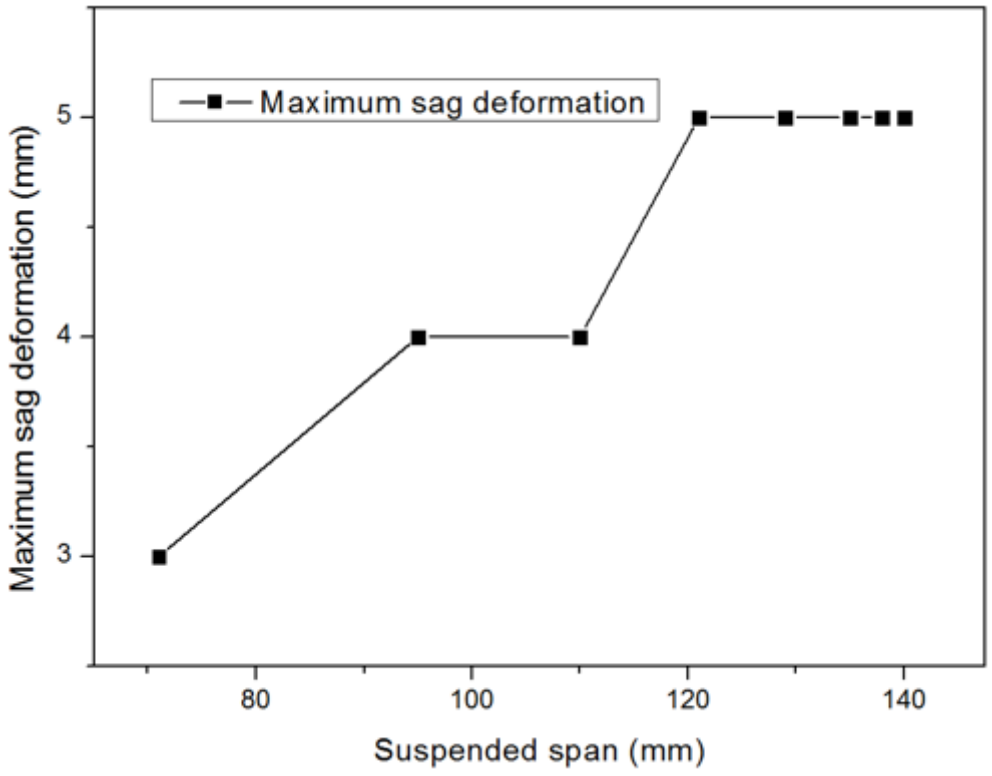

Figure 12

Sagging deformation of suspended monofilament under different spans

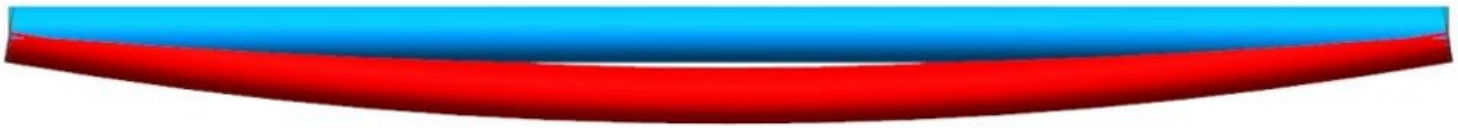

Figure 13

Contact areas between the second layer monofilament and the first layer at 71mm span

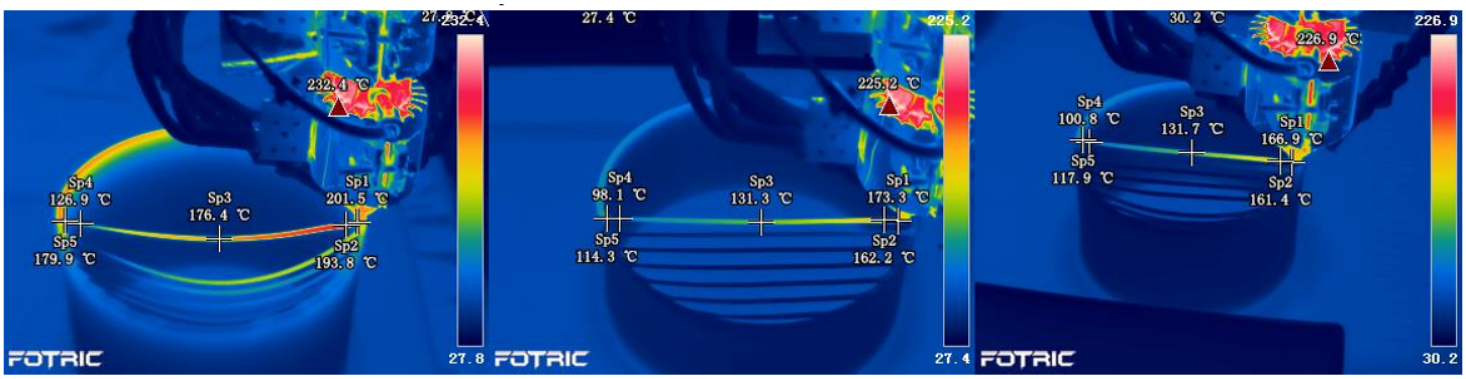

Figure 14

Thermal field diagrams

a D=200mm, v=70mm/s, air cooling b D=200mm, v=20mm/s, air cooling c D=150mm, v=20mm/s, air cooling

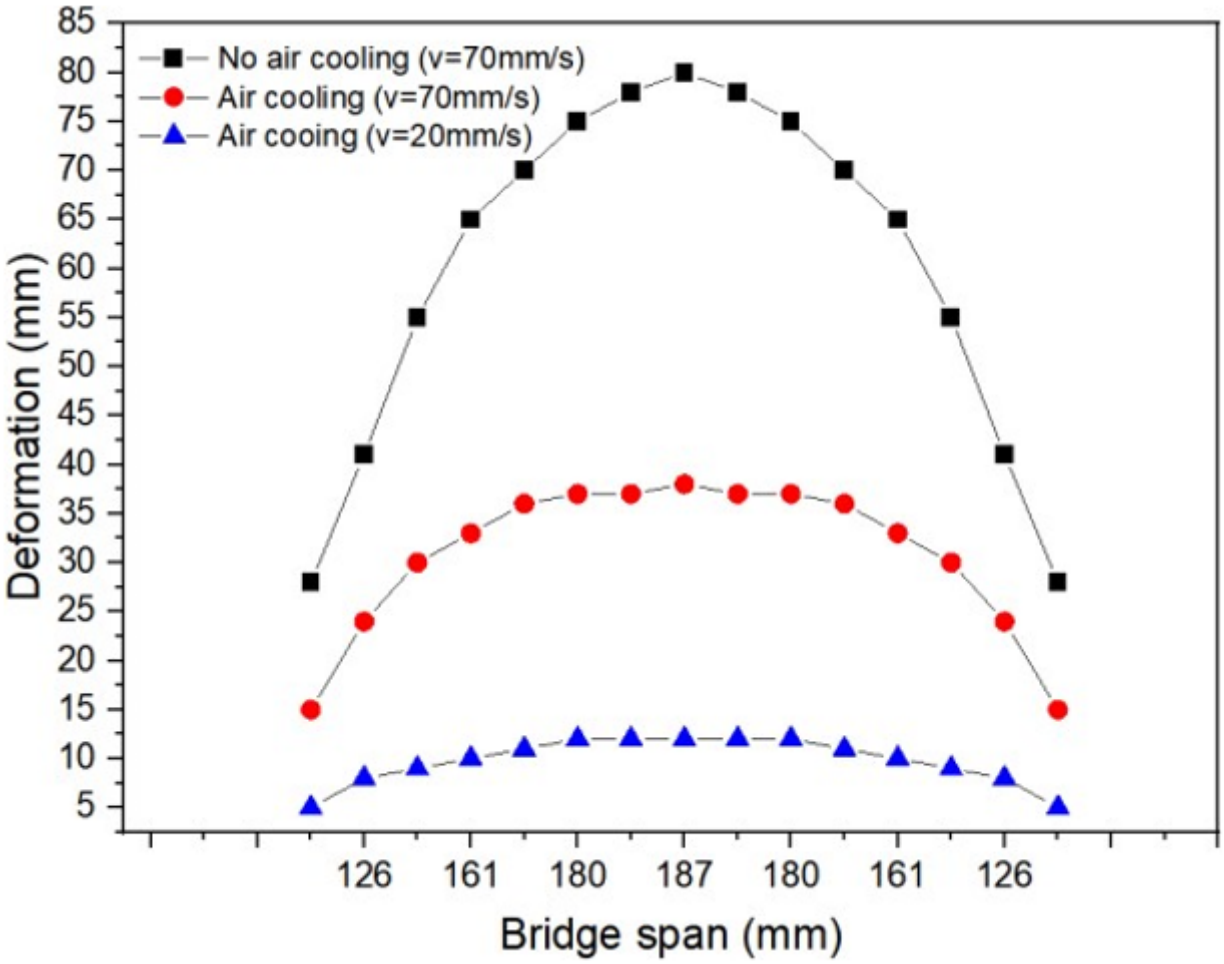

Figure 15

Comparison of deformation under different cooling States (D=200mm)